Supporting Information

Influence of three-dimensional nanoparticle branching on the Young's modulus of polymer-nanocomposites: Effect of interface orientation

Shilpa N. Raja[1,2], *Andrew C. K. Olson*[3]*[†], *Aditya M. Limaye*[4]*, *Kari Thorkelsson*[1,2††], *Andrew J. Luong*[4], *Liwei Lin*[5], *Robert O. Ritchie*[1,2,5], *Ting Xu*[1,2,3] *A. Paul Alivisatos*[1,2,3,6]^

[1]Materials Sciences Division, Lawrence Berkeley National Laboratory, Berkeley, California, 94720, U.S..

[2]Department of Materials Science and Engineering, University of California, Berkeley, Berkeley, California, 94720, U.S.

[3]Department of Chemistry, University of California, Berkeley, Berkeley, California, 94720, U.S.

[4]Department of Chemical Engineering, University of California, Berkeley, Berkeley, California, 94720, U.S.

[5]Department of Mechanical Engineering, University of California, Berkeley, California, 94720, U.S.

[6]Kavli Energy NanoScience Institute, Berkeley, California 94720, U.S.

^Corresponding Author (apalivisatos@lbl.gov)

*These authors contributed equally.

[†] Current Address: ZS Associates, San Francisco, CA, U.S.

[††] Current Address: Lam Research, Livermore, CA, U.S.

S1. LSM Simulations of the Polymer Nanocomposites

An alternative to finite element models[1], elastic lattice spring models (LSMs) model a material as an elastic spring network to estimate the Young's modulus. Elastic LSMs have been shown to reproduce the equations of state for an isotropic elastic medium in the case of small deformations[1]. The LSM used in this work was a two-dimensional model identical in form to the LSM in a previous study[2]. Although LSMs which model plastic deformation also exist[2], the LSM used in the present study accounted only for small-displacement (less than ~1%) fully elastic deformations[3].

SI Figure 8 illustrates the data structure for the lattice spring model used in the simulations. It consists of a simple square lattice (we refer to each lattice point here as a "node") of a network of one-dimensional, Hookean springs connecting nearest and next-nearest neighbors (chosen to be homogeneous to represent the amorphous SEBS matrix in our experimental study[4]). Nano-reinforcements tQDs and NRs had a width of 3 nodes. Each arm of the tQD was 14 nodes long, as was each NR. The nanometer-node equivalency (the number of nodes in the LSM corresponding to nanometers in the nanocomposites) for width was 1.67 nm/node for rods and tetrapods and 0.4 nm/node for dots. For lengths, the ratio was 1.78 nm/node for rods and tetrapods. Changes in nanometer-node equivalencies for lengths between 0.4 to 3 were found to have no impact on results as long as fill factor was kept the same. Furthermore, each particle was surrounded by a one-node wide interface region represented by nodes with a spring constant of 0.5. Tests for NRs and tQDs were all conducted with a constant matrix size of 156x156 nodes, while dipod matrix sizes varied from 48x48 to 52x52 nodes. The matrix size was not found to affect the calculations, though smaller matrices were used to decrease computational times.

In order to properly represent physical conditions, a number of guiding assumptions were made regarding the placement and spring constants of nanoparticles in the lattice spring model. Consistent with previous work[5] as well as transmission electron microscopy (TEM) images of samples in this study (Fig. 2), the tetrapod quantum dots (tQDs) were dispersed in porous and loosely packed aggregates. This was anticipated based on previous theoretical studies of nanoparticle superstructure, which indicated that tQDs are likely to remain kinetically arrested in a glassy superstructure due to their multiple arms. Nanorod (NR) aggregates, on the other hand, were closely packed, as demonstrated previously[1]. Each NR was "interdigitated", separated solely by two ligand nodes rather than polymer nodes. Much like tQD nanocomposites, however, simulations revealed that the modulus of NR nanocomposites had little to no dependence on the packing density of the NRs (SI Fig. 3).

Due to the two-dimensional nature of the LSM, area-fill factors obtained from TEM image analysis of our nanocomposites were used for comparison to experimental results rather than using experimental volume fill factors. This was required to achieve good agreement between experiment and theory and is justified by a geometric analysis, which reveals that the 2D and 3D area and volume fill factors differ in two *vs*. three dimensions, with the difference being equal to the ratio of the heights of the polymer and aggregate cylinder. Since these values are unknown, the percentage of nodes assigned as nanoparticle nodes was chosen to identically match the cross-sectional area fill factors (*i.e.*, how much of the TEM image was taken up by nanoparticle aggregates) from a TEM image analysis of our nanocomposites (these matched the weight percents (Fig. 2)). This is justified by two observations. First, a vast majority of our aggregates (Fig. 2) were much larger in size than the microtomed TEM cross-sections (~60 nm), meaning that the images are an accurate 2D representation of our aggregates. Second, due to elongation in the tensile direction during electrospinning, the fibers are approximately cylindrical, meaning that the cross-sectional area fill factor is approximately uniform throughout the fiber length.

After the NPs were placed in the polymer matrix, a tensile stress was applied and the purely elastic strain field corresponding to the lowest energy configuration of the lattice springs was calculated, as well as the Young's modulus and Poisson's ratio. Since the model is deterministic, only one trial was used for each simulation of tetrapods and quantum dots. For rods, two deterministic simulations were performed at each opposing orientation (oriented fully with and against the tensile axis) and the average of these was taken to determine the Young's modulus. Force was applied at the boundary nodes. Spring constants between nodes of different (polymer, nanoparticle, or interface) regions were defined as the average of the different nodes.

The good agreement between experimental results and theoretical LSM predictions was based on non-arbitrary physical assumptions, such as the experimentally-obtained fill factor (from TEM image analysis) and experimentally derived ratios for the nanoparticle and polymer spring constants. The only other variables, the interface spring constant and width, were selected based on experimental ratios for ligand length and nanoparticle size, and the similarity of the ligand shell with poly(ethylene-butylene) (PEB). Changing the value for interface strength did not lead to significant deviations from experimental values when the interface value was within a factor of two of the polymer spring constant (SI Fig. 6).

Finally we note that purely elastic LSMs, as utilized here and in previous NP-polymer studies,[6] are not perfect models. Since the springs in the LSM are elastic, they are limited in their scope to modeling situations where the displacements are small. Simulation of the nanoparticle-polymer interface comprises an active area of research; the structure of the interface is contested, resulting in uncertainty when simulating the interface. Finally, the conformational entropy of individual polymer chains, which forms the basis for many theories of chain deformation[7], is not accounted for in deriving the elastic energy.

S2. Results on Film Composites

After initial experiments with electrospun fiber matrices, all the experimental results on mechanical testing of composites in this work were reproduced on solvent-cast bulk films of ~100 μm thickness. In the bulk format, the SEBS polymer used in this work is widely employed in everything from sports equipment to electronics. These results are shown in SI Figs. 1 and 5, which illustrate, respectively, mechanical data and TEM characterization on these films. Details of their preparation are described in the Methods section of the main text. We have found that the nanoparticle dispersion and shape dependence of the Young's modulus for NR- and tQD-based composites roughly matches that of the electrospun fibers within ~10%, with slightly less scatter in the Young's modulus (a factor of ~1.5 less scatter in the raw data). The phase-separated nanoparticle dispersion in these bulk films is roughly similar to that of the electrospun fibers, as shown in SI Fig. 5. Since the scatter is only slightly less across 8-9 samples, this suggests that part of the scatter that we see may be due to nanoparticle aggregation, while part may be due to electrospinning structural variations.

S3. Ligand Coverage Differences Between tQDs and NRs

Our analytical estimates using a ‘triangle of frustration’ between the arms defined by the ligand interdigitation length give a difference in ligand coverage density of 8-9% between tQDs and NRs for the native octadecylphosphonic acid (ODPA) ligands[8]. The small 8-9% decrease for tQDs is due to the fact that the junctions between the tQD arms reduce the amount of space for ligands to interdigitate, and so below the ligand interdigitation distance (3.4 nm for ODPA[9]) it is likely that ligand coverage is far less due to the inability of adjacent chains to interdigitate. At the weak interface that comprises our native ligands (roughly half the modulus of the polymer, according to our interface fits in SI Fig. 6), we find that varying the percent of the 2D matrix occupied by the ligand from 4-9% makes less than ~1% difference in the obtained stiffnesses. Therefore, we conclude that the native ligand case is a fair comparison between the shapes.

S4. Simulations on Nanocomposite Stiffness as a Function of Aggregate Volume Fraction (Area Fraction in 2D)

We have conducted simulations, included here in the SI, to study the effect of volume fraction (area fraction in 2D) on the Young’s modulus for tQDs, NRs, and dipods, varying the volume fraction (area fraction in 2D) of the aggregate from ~<20-90% at constant nanoparticle fill factor and constant interface width and stiffness. Like tetrapods in 3D, dipods in 2D can approach arbitrarily close, as can interdigitated rods. We found that across the three 2D shapes studied that there was no significant change in the stiffness (only a 2-6% change, (SI Table 3 and SI Figs. 3-4), as compared to 30-150% across shapes at the different concentrations studied). The effect of aggregate area fraction in our 2D lattice spring model is minimal compared to the shape-dependent effects on stiffness. As explained in the main text in the Discussion section, we believe that this is because at the very small displacements below the elastic limit, the polymer trapped in between the tQD aggregates does not get displaced enough for its restricted area to affect the overall stiffness (analogous to electrical cables entangled in a knot, which simply slide before the knot tightens).

S5. Using 2D Simulations for 3D Nanocomposites

We have used a 2D LSM approach in this work, despite the fact that the tQD is an inherently 3D object. However, we feel our results and our interface orientation argument qualitatively hold regardless of dimension. There is established body of literature which has investigated the potential of 2D LSMs to simulate 3D particle polymer composites[10,11], where qualitative comparisons have been conducted between 2D simulated results with those expected from a 3D case[11]. Notably, Bohm and Han[12] analyze some 9 different 2D and 3D models and demonstrated that they differ in the computed elastic modulus in 2D and 3D by only ~5-10% percent.

S6. Experimental Materials and Methods

Note: Since many of the methods used here were identical to the methods we used previously[13], they are replicated below with small changes.

Materials

All chemicals used were purchased from Sigma Aldrich. SEBS polymer was kindly provided by Kraton corporation (MD1537, white powder).

Synthesis of CdSe-CdS Tetrapods, CdSe-CdS Nanorods, and CdSe Quantum Dots.

Heterostructured CdSe-CdS core/shell tQDs and NRs were synthesized and cleaned as reported previously[14]. All shapes had the same or similar alkyl chain ligand surface chemistry; tQDs and NRs were coated with octadecylphosphonic acid and trioctylphosphine oxide. The tQDs used had an arm length of 28.0 ± 4.8 nm and an arm diameter of 4.5 ± 0.8 nm and the NRs used had an average length of 31.5 ± 15.0 and an average arm diameter of 4.9 ± 0.8.

Preparation of Nanoparticle-Polymer Precursor Solutions for Electrospinning and Film Casting.

Chloroform solutions containing appropriate concentrations of native tQDs or NRs were mixed with premade polymer-chloroform solutions to create solutions of 12% SEBS by weight in chloroform with 5%, 10%, and 20% nanoparticle incorporation by weight of polymer. Solutions were typically made with 25 mg SEBS polymer and about 0.5 mL of chloroform in order to achieve the high viscosity needed for electrospinning. Due to the excellent solubility of the polymer in chloroform, dissolution was observed to occur within minutes. Regardless, solutions were vortexed for several hours to ensure uniformity. Thin film composites of SEBS were prepared by casting mixed solutions of nanoparticles and SEBS in chloroform (~140 mg SEBS in ~8 mL of chloroform) into glass petri dishes and allowing the films to dry in a fume hood before further drying overnight under vacuum.

Electrospinning of Tetrapod-SEBS Composite Single Fibers.

Electrospinning was performed using a bias of 15 kV between the collector and syringe needle and collector-syringe needle distance of 150 mm for all runs (electric field of 1 kV/cm) For all samples, needles purchased from Nordson Corporation (part number 7018225, #21 gauge, 38.1 mm gauge length, 0.51 mm inner diameter) were used. Approximately 0.1-0.2 mL of solution was loaded into the syringe, and a large droplet of solution was manually ejected immediately prior to turning on the power supplies.

Chloroform (Sigma Aldrich) was used as the electrospinning solvent.

Single fibers of diameter 1-6 um were fabricated using the collector design of Li *et al*. (3), consisting of two metal rods of 8 mm diameter spaced 95 mm apart, while dynamic scanning calorimetry (DSC) samples were fabricated using a random fiber network deposited onto a single metal rod under the same electric field conditions. Electrospinning was conducted in a fume hood set to low flow to avoid damage and entanglement of fibers. Care was taken to ensure identical conditions of voltages, distances, and air flow for all electrospinning rounds. For transmission electron microscopy (TEM) studies, single aligned fiber arrays were wound around a microtomable epoxy substrate and sputter-coated with 15 nm of gold. Single fibers were removed from the double-rod collector using twisted pipe cleaners coated with double-sided tape, and subsequently taped and glued directly onto cardboard tabs with diamond-shaped cutouts for mechanical tests. In order to compare mechanical properties between shapes, all aspects of the nanocomposites except nanoparticle shape were kept constant – volume fractions, sample preparation, electrospinning parameters, and mechanical testing parameters such as strain rate.

Tensile Testing and Diameter Measurements on Fibers and Films

Single fibers in an aligned array were removed from the double-rod collector using twisted pipe cleaners coated with double-sided tape, and subsequently taped and glued with epoxy directly onto small cardboard tabs (10 mm x 5 mm) with diamond-cut openings for mechanical tests. Samples were dried for several hours prior to mechanical testing. Care was taken to minimize damage to fibers during collection. However, variation in fiber structure[15], as before, may arise from varying electric fields along the double-rod collector[13,15], as well as variations in nanoparticle dispersion in the polymer. The diameters of the fibers were imaged and photographed using a 63x objective lens on a standard optical microscope (QCapture camera and QImaging software) which was calibrated using a TEM grid (17.97 pixels/um). The fiber diameters were analyzed using ImageJ. The thickness and width of bulk films (~100 um in thickness, ~1-2 mm in width) were assessed using digital calipers. Uniaxial tensile testing was performed using an Agilent T150 nanomechanical tensile tester. The strain rate was set to $6.9x\ 10^{-3}$ for all fiber runs and 10×10^{-3} for all film runs, and film strips and fibers glued to tabs were mounted in the tensile tester using standard pivot grips. The average fiber diameter measured over 20-25 samples was around 4 μm ± 1 μm for all nanoparticle shapes tested. The gauge lengths, measured with digital calipers, fell between 6-10 mm for fibers and 1-3 mm for films. No dependence of the Young's modulus on the gauge length was found for either set of samples. For standard tensile mechanical tests, we conducted a total of 14-25 tests per fiber sample of 0%, 5%, 10%, and 20% loading by weight of tetrapods and rods, and 8-9 tests for each film data point. In order to obtain the Young's moduli, linear trendlines were fit to the curve points in the linear elastic region. Data were carefully evaluated to rule out a diameter dependence on mechanical testing.

Transmission Electron Microscopy Imaging and Sample Preparation.

Electrospun fiber mats and/or films of polymer nanocomposites were deposited onto microtomable epoxy substrates and then embedded in epoxy stained with rhodamine 6G and cured overnight at 60°C. An ultramicrotome was used to cut ~60 nm thin sections, which were floated onto copper TEM grids from water. These sections were then imaged in a FEI Tecnai 12 TEM at an accelerating voltage of 120 kV or a FEI Tecnai G2 at 200 kV. For films, ~70 nm sample sections were obtained by cryo-microtoming at -110 to -120°C.

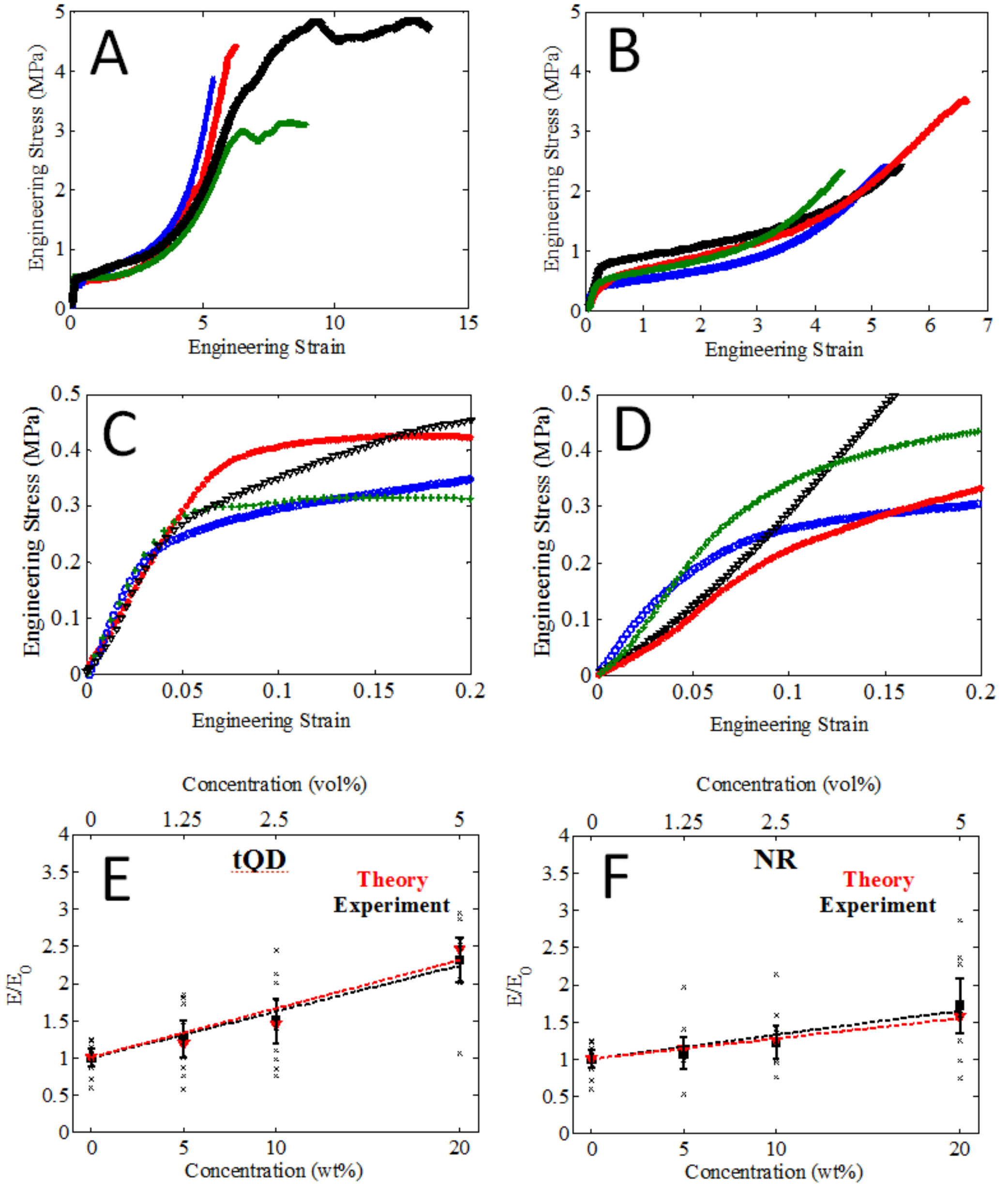

SI Figure 1. Comparison of Experimental Results on Bulk SEBS Films with Simulated Data Using Lattice-Spring Model. (A) Example mechanical curves to failure of 20% tQD-SEBS nanocomposite films. (B) Example mechanical curves to failure of 20% NR-SEBS nanocomposite films. (C) Example mechanical curves of 20% tQD-SEBS nanocomposite films, shown over the first 0.2 strain to highlight the elastic region. (D) Example mechanical curves of 20% NR-SEBS nanocomposite films, shown over the first 0.2 strain to highlight the elastic region. Top x-axis is volume percent concentration, while bottom x-axis is weight percent. (E) Plot of Young's modulus (E), normalized to control modulus (E_0) versus nanoparticle concentration for tQD-SEBS film nanocomposites. (F) Plot of Young's modulus (E), normalized to control modulus (E_0) versus nanoparticle concentration for NR-SEBS film nanocomposites. Red lines/points represent results from the lattice-spring model, while black lines/points represent experimental results. Each black "x" is the result of a single experimental test. Linear fits are clamped to the (0,1) point which corresponds to the normalized control modulus.

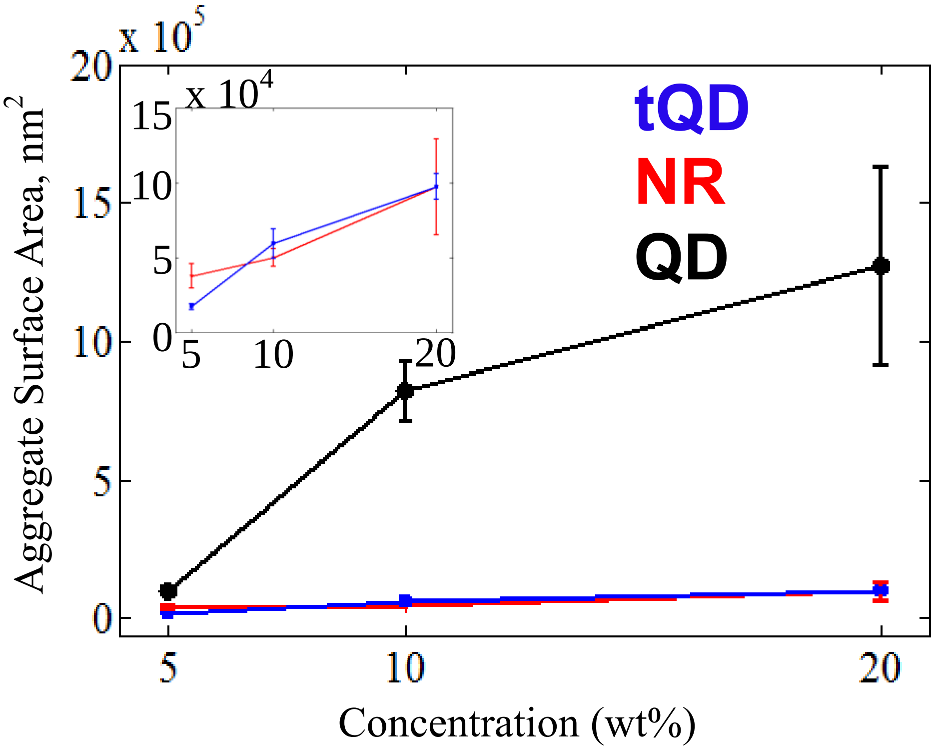

SI Figure 2. Aggregate Surface Area in Polymer Nanocomposites: Plot depicts the average aggregate surface areas as determined from a size analysis on TEM images of microtomed polymer nanocomposites. Inset shows greater detail for tQDs and NRs.

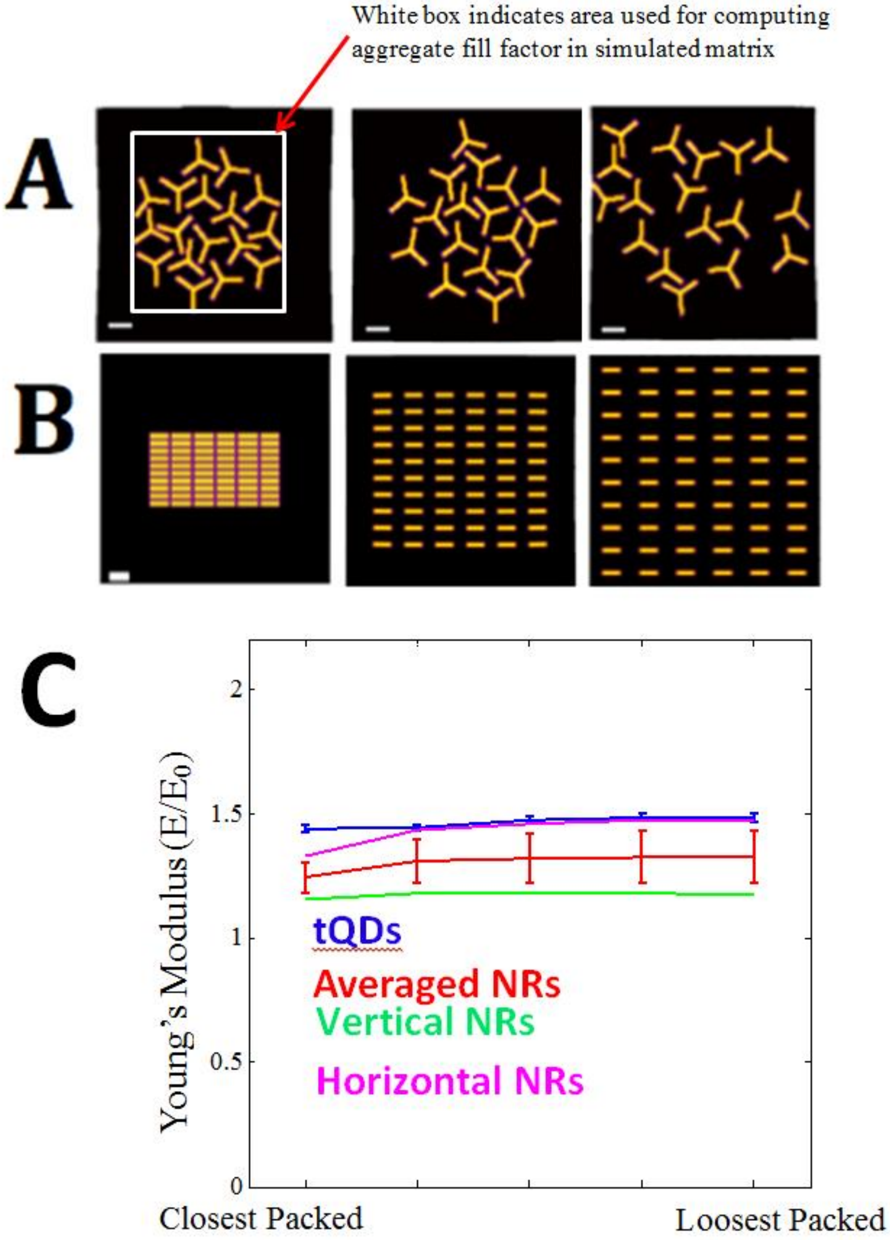

SI Figure 3. Polymer Nanocomposite Modulus as a Function of Packing. (A) Images of tQD aggregates studied with decreasing packing (left to right). The white box indicates the area used in computing the aggregate fill factor. (B) Corresponding image for horizontal NRs. Five total packings were studied. Scale bars are 25 nm for all images, and all images are to the same scale. (C) Plot of Young's modulus (E/E_0) *vs*. packing for NR and tQD nanocomposites. Blue line represents averages of over 12 trials of randomly placed tQDs while the red line represents the average of vertical (green) and horizontal (magenta) NR. All simulations shown in SI Figure 3 used a nanoparticle area fill factor of 10%, held constant across all stiffness vs. packing simulations. The aggregate fill factor, defined as the area taken up by the entire aggregate, was varied in SI Figure 3 from 18.5% to 80.5% for NRs and 48.3% to 83.0% for tQDs (closest and loosest packed, respectively; the middle packing was at 51.3% for NRs and 73.2% for tQDs).

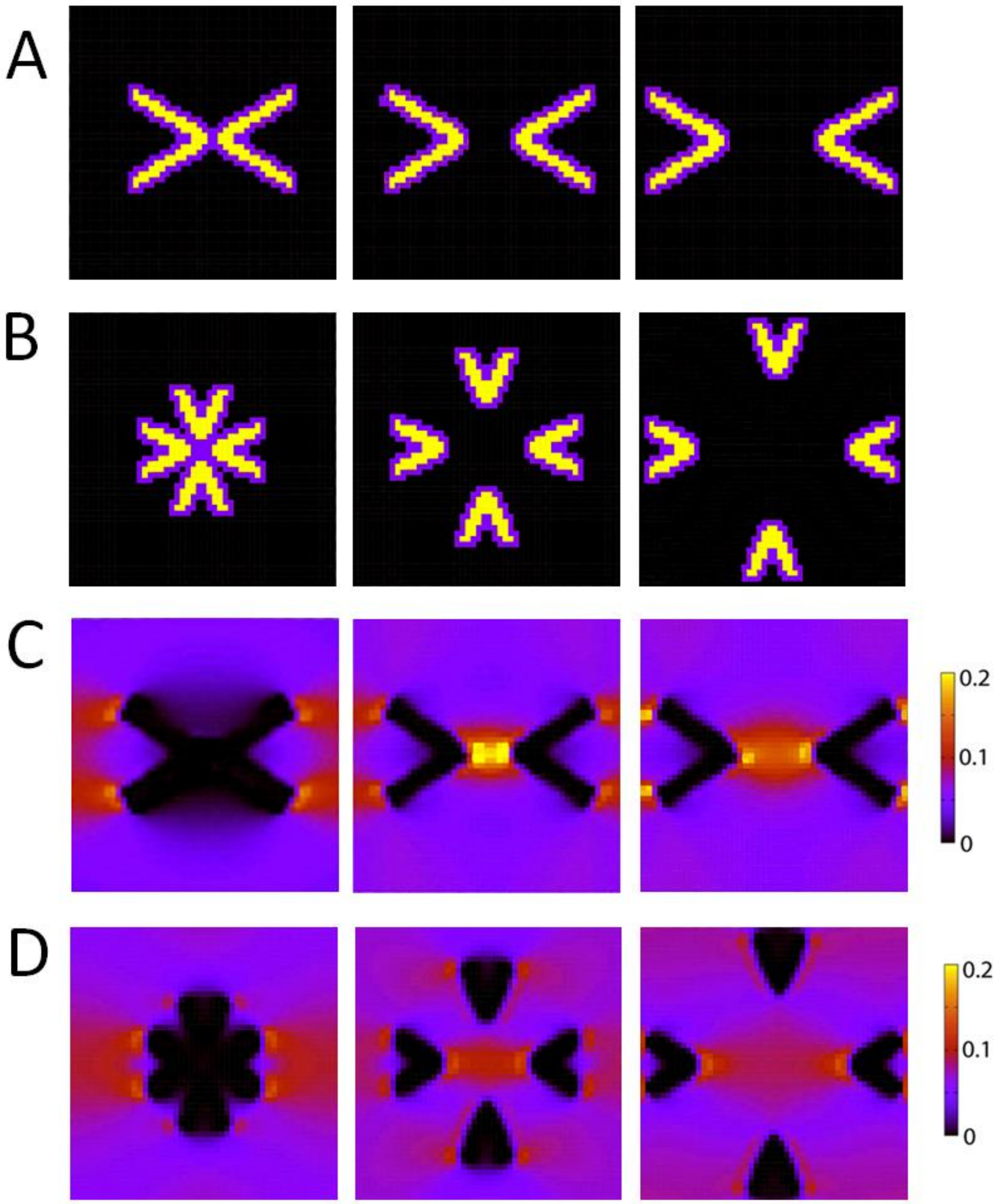

SI Figure 4. Studies of Aggregate Area Fraction Occupied by Two Geometries of Dipods on the Young's Modulus. A. Mask (input, or spring distribution) files for 2 dipods flipped 180 degrees with respect to each other. B. Mask files for 4 dipods arranged orthogonally. C. Strain distribution images for input files in A. D. Strain distribution images for input files in B. For stiffness changes, see SI Table 2.

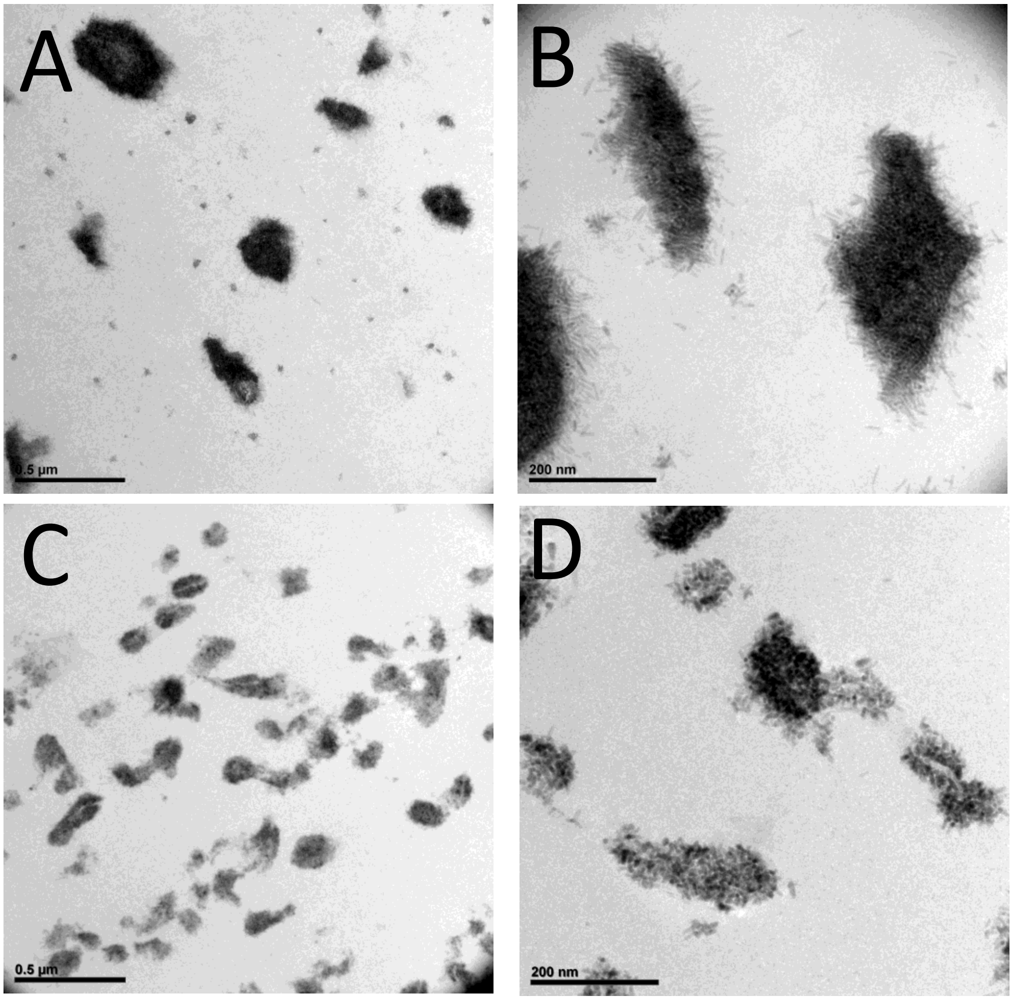

SI Figure 5. Transmission Electron Micrographs of tQD and NR Film SEBS Polymer Nanocomposites. (A) Wide-area micrograph of 20% NR-SEBS nanocomposites. (B) Close-area micrograph of 20% NR-SEBS nanocomposites. (C) Wide-area micrograph of 20% tQD-SEBS nanocomposites. (D) Close-area micrograph of 20% tQD-SEBS nanocomposites. Scale bars are 500 um (A, C) and 200 um (B, D).

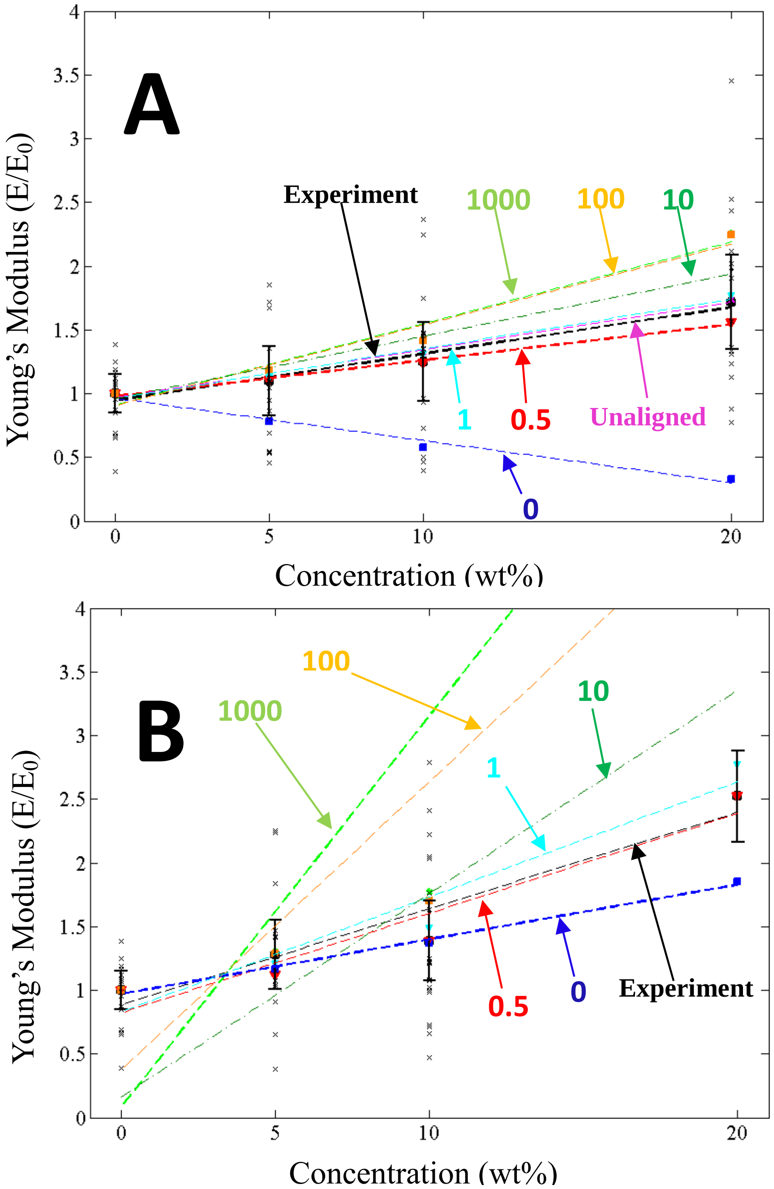

SI Figure 6. Effect of Varying Interfacial Spring Constant: Effect of varying the interfacial spring constant on the nanocomposite Young's modulus for (A) NR nanocomposites and (B) tQD nanocomposites.

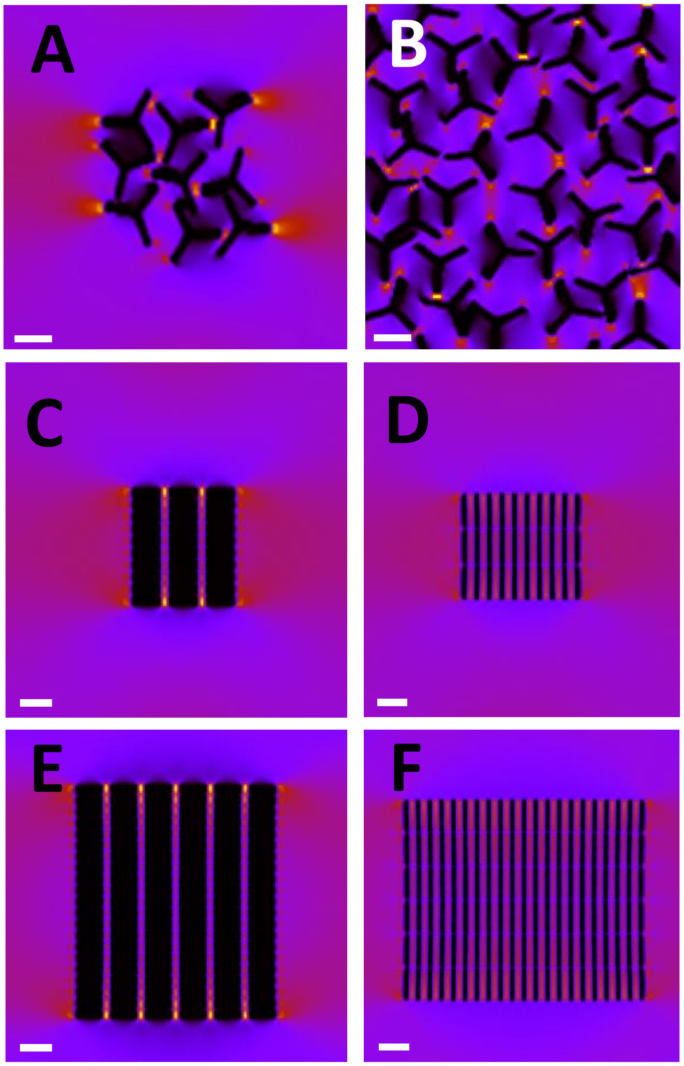

SI Figure 7. Simulated Strain Fields of tQD and NR Nanocomposites: (A) 5 wt.% tQD-SEBS composites; (B) 20 wt.% tQD-SEBS composites; (C) 5 wt.% horizontal NR-SEBS composites; (D) 5 wt.% vertical NR-SEBS composites; (E) 20 wt.% horizontal tQD-SEBS composites and (F) 20 wt.% vertical NR-SEBS composites. Scale bars are 25 nm (14 nodes) for all NR and tQD images.

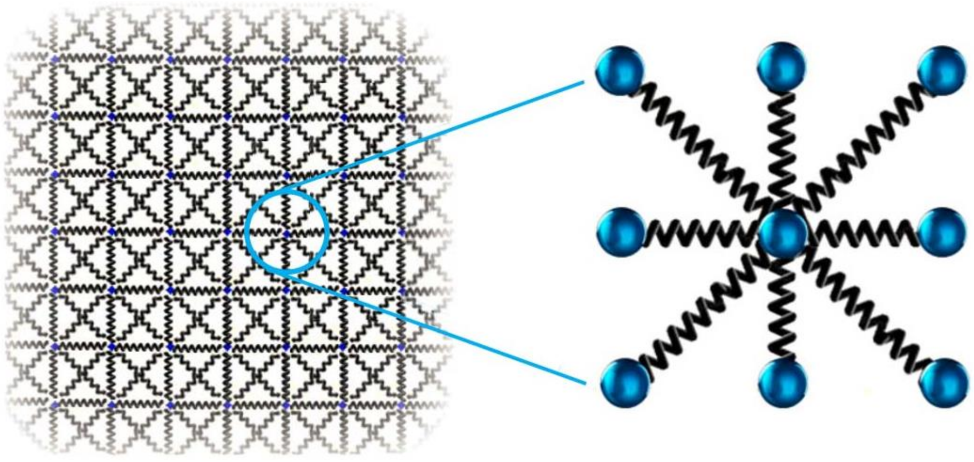

SI Figure 8. LSM Schematic: A schematic illustration of the LSM used in this study, with a simple square lattice and springs connecting nearest and next-nearest neighboring lattice points.

	Parameter	NR fibers	tQD fibers	NR films	tQD films
Experimental Fits	A	0.0330	0.0680	0.0322	0.0617
	B	1.0	1.0	1.0	1.0
Theoretical Fits	A	0.0272	0.0655	0.0272	0.0655
	B	1.0	1.0	1.0	1.0

SI Table 1. Trendline Fits: Slopes (A) and intercepts (B) for the linear fits (fits are clamped to the 0,1 data point) shown in Fig. 4 and SI Fig 1. Goodness of fit (R^2) varied between ~0.95 to ~0.99 for NRs and tQDs respectively in both fibers and films.

Packing	Structure (see SI Fig. 4)	Aggregate Area Fill Factor	Nanoparticle Fill Factor	% Change in Stiffness
Closest Aggregate Packing (5.5c for instance, insert these later once re-ordered everything)	90 Dipods	24.0%	10%	0
Intermediate Packing	90 Dipods	52.6%	10%	6.0%
Loosest Packing	90 Dipods	92.3%	10%	6.0%
Closest Packing	180 Dipods	32.8%	10%	0
Intermediate Packing	180 Dipods	35.6%	10%	4.1%
Loosest Packing	180 Dipods	43.8%	10%	2.7%

SI Table 2. Stiffness as a function of aggregate packing for dipods with aggregate fill factor in the 2D matrix ranging from 24.0% to 92.3%. (See SI Fig. 4 for images corresponding to these packings). The last column of percent changes in stiffness are defined relative to the closest packed composite. The structure '90 dipods' refers to 4 dipods arranged orthogonally, while '180 dipods' refers to 2 dipods as shown in SI Fig. 4.

Importance of Variable for Nanoparticle Type (Y = Important, N = Unimportant/Minimal Effect)	tQDs	NRs
Placement Angle (in Close-Packed Aggregate)	No	Yes
Interfacial Bond Strength	Yes	Yes
Cavity Shape/Size/Position	N/A	N/A
Aggregate Packing Density	No	No

SI Table 3. Summary of Effects of Specific Parameters on the Results of the Simulations.

References

1. Ostoja-Starzewski, M. Lattice Models in Micromechanics. *Appl. Mech. Rev.* **2002**, *55*, 35-60.
2. Buxton, G. A.; Care, C. M.; Cleaver, D. J. A Lattice Spring Model of Heterogeneous Materials with Plasticity. *Modelling Simul. Mater. Sci. Eng.* **2001**, *9*, 485–497.
3. Buxton, G. A.; Balazs, A. C. Lattice Spring Model of Filled Polymers and Nanocomposites. *The Journal of Chemical Physics* **2002**, *117*, 7649–7658.
4. Sierra, C. A.; Galan, C.; Fatou, J. G.; Parellada, M. D.; Barrio, J. A. Thermal and Mechanical Properties of Poly (Styrene- B-Ethylene- Co-Butylene- B-Styrene) Triblock Copolymers. *Polymer* **1997**, *38*, 4325-4335.
5. Blaak, R.; Mulder, B. M.; Frenkel, D. Cubatic Phase for Tetrapods. *The Journal of Chemical Physics* **2004**, *120*, 5486-5492.
6. Dair, B. J.; Honeker, C. C.; Alward, D. B.; Avgeropoulos, A.; Hadjichristidis, N.; Fetters, L. J.; Capel, M.; Thomas, E. L. Mechanical Properties and Deformation Behavior of the Double Gyroid Phase in Unoriented Thermoplastic Elastomers. *Macromolecules* **1999**, *32*, 8145–8152.
7. Buxton, G.; Balazs, A. C. Simulating the Morphology and Mechanical Properties of Filled Diblock Copolymers. *Phys. Rev. E* **2003**, *67*, 031802.
8. Anderson, N. C.; Hendricks, M. P.; Choi, J. J.; Owen, J. S. Ligand Exchange and the Stoichiometry of Metal Chalcogenide Nanocrystals: Spectroscopic Observation of Facile Metal-Carboxylate Displacement and Binding. *Journal of the American Chemical Society* **2013**, *135*, 18536-18548.

9. Baker, J. L.; Widmer-Cooper, A.; Toney, M. F.; Geissler, P. L.; Alivisatos, A. P. Device-Scale Perpendicular Alignment of Colloidal Nanorods. *Nano Letters* **2009**, *10*, 195-201.
10. Ostoja-Starzewski, M. Lattice Models in Micromechanics. *Applied Mechanics Reviews* **2002**, *55*, 35-60.
11. Zhu, G.; Alexeev, A.; Kumacheva, E.; Balazs, A. C. Modeling the Interactions Between Compliant Microcapsules and Pillars in Microchannels. *The Journal of Chemical Physics* **2007,** *127*, 034703.
12. Böhm, H. J.; Han, W. Comparisons Between Three-Dimensional and Two-Dimensional Multi-particle Unit Cell Models for Particle Reinforced Metal Matrix Composites. *Modelling and Simulation in Materials Science and Engineering* **2001**, *9*, 47-65.
13. Raja, S. N.; Olson, A. C. K.; Thorkelsson, K.; Luong, A. J.; Hsueh, L.; Chang, G.; Gludovatz, B.; Lin, L.; Xu, T.; Ritchie, R. O.; Alivisatos, A. P. Tetrapod Nanocrystals as Fluorescent Stress Probes of Electrospun Nanocomposites. *Nano Lett.* **2013,** *13*, 3915–3922.
14. Talapin, D. V.; Nelson J. H.; Shevchenko E. V.; Aloni, S. Seeded growth of highly luminescent CdSe/CdS nanoheterostructures with rod and tetrapod morphologies. *Nano Lett.* **2007,** *7*, 2951-2959.
15. Deitzel J. M.; Kleinmeyer, J.; Harris, D. E. A.; Tan, N. C. B. The effect of processing variables on the morphology of electrospun nanofibers and textiles. *Polymer* **2001,** *42*, 261-272.